

# Bounding Dark Energy from the SPARC rotation curves: Data driven probe for galaxy virialization

David Benisty,<sup>1,2,\*</sup> David Vasak,<sup>1,†</sup> Jürgen Struckmeier,<sup>1,‡</sup> and Horst Stoecker<sup>1,3,4,§</sup>

<sup>1</sup>Frankfurt Institute for Advanced Studies (FIAS), Ruth-Moufang-Strasse 1, 60438 Frankfurt am Main, Germany

<sup>2</sup>Helsinki Institute of Physics, P.O. Box 64, FI-00014 University of Helsinki, Finland

<sup>3</sup>Fachbereich Physik, Goethe-Universität, Max-von-Laue-Strasse 1, 60438 Frankfurt am Main, Germany

<sup>4</sup>GSI Helmholtzzentrum für Schwerionenforschung GmbH, Planckstrasse 1, 64291 Darmstadt, Germany

Dark Energy (DE) acts as a repulsive force that opposes gravitational attraction. Assuming galaxies maintain a steady state over extended periods, the estimated upper bound on DE studies its resistance to the attractive gravitational force from dark matter. Using the SPARC dataset, we fit the Navarro-Frenk-White (NFW) and Hernquist models to identify the most suitable galaxies for these models. Introducing the presence of DE in these galaxies helps establish the upper limit on its repulsive force. This upper bound on DE sits around  $\rho_{(<\Lambda)} \sim 10^{-25} \text{ kg/m}^3$ , only two orders of magnitude higher than the one measured by Planck. We discuss the conditions for detecting DE in different systems and show the consistency of the upper bound from galaxies to other systems. The upper bound is of the same order of magnitude as  $\rho_{200} = 200\rho_c$  for both dark matter profiles. We also address the implications for future measurements on that upper bound and the condition for detecting the impact of  $\Lambda$  on galactic scales.

## I. INTRODUCTION

DARK ENERGY is an unknown form of energy that affects the universe on the largest scales [1]. Its primary effect is to drive the accelerating expansion of the universe. The first observational evidence for DE's existence came from measurements of supernovae [2, 3]. Besides this, Baryon Acoustic Oscillations (BAO) [4–7] and the Cosmic Microwave Background (CMB) [8] give a strong evidence for the need to modify either the matter sector of the universe or the gravitational sector. Dark matter is another dominant part in our Universe as its density is about five times larger than the baryon matter density. Its postulation is motivated by observations of the dynamics of galaxies and their flat rotation curves [9]. Without dark matter the slope of the rotation curve, which is the plot of the orbital velocities of visible stars or gas in a galaxy vs. their radial distance from the center, would be much steeper.

From the observation of different galaxies like Andromeda, the Milky Way [10–12], dwarf galaxies and others [13–31], a universal density profile, now known as the Navarro-Frenk-White (NFW) model that grows at small radii like  $\rho \sim r^{-1}$  and behaves as  $\rho \sim r^{-3}$  for large radii, was first suggested in Ref. [32]. Subsequent work, though, weakened the universality of that model and proposed alternative density profiles [33–39].

Modified Gravity (MoG) can mimic the dark matter components [40–42]. For example the Modified Newtonian Dynamics (MOND) model was explicitly designed to explain the flatness of rotation curves [43–45]. It modifies Newton's second law at low accelerations and recovers

the Tully-Fisher relation without introducing additional dark matter [46–51]. Another ansatz for modified gravity is to define a different potential at the low energy limit by integrating over the dark matter model [52–54]. Tests of MoG have been carried out using a variety of probes from the kinematics of stars and gas in the Milky Way [55] through the fundamental plane of elliptical galaxies [56] to galaxy rotation curves [57–59].

Although dark energy, represented by the cosmological constant  $\Lambda$ , dominates at cosmological scales, it is also effective on the scale of the local Universe [60–77]. In the low energy regime it modifies the Newtonian potential in the equation of motion of a star on a circular orbit around a central mass  $M$  to

$$\frac{\ddot{r}}{r} = -G\frac{M}{r^3} + \frac{\Lambda c^2}{3}. \quad (1)$$

Here  $r$  is the distance of the star to the mass center,  $G$  is the Newtonian gravitational constant, and  $c$  is the speed of light. As shown in Ref. [76, 78], the impact of dark energy can indeed be observed also in the local Universe when the Milky Way and the M31 galaxy are considered as a binary system. In this paper, we wish to assess for the first time the influence of dark energy on galaxy rotation curves, and estimate an upper bound on the cosmological constant. We show that albeit DE is naturally related to a length scale, there is a strong correlation between the upper bound of DE and the galaxy scaling density. That scale of galaxies is about  $r \sim \text{Kpc}$ , hence one would expect that the upper bound on DE should be around  $\Lambda < 1/\text{Kpc}^2 \sim 10^{-36} \text{ m}^{-2}$ . However, in the paper, we show that the upper bound on  $\Lambda$  corresponds to the virial critical density  $\rho_{200}$  of the galaxy, which gives a range of  $\Lambda < 10^{-48} \text{ m}^{-2}$  (with  $\hbar = c = 1$ ), much closer to the cosmological value than expected previously. These bounds are compatible with other DE probes [78, 79].

As Ref. [78] shows, for the lower curvature of the system, the upper bound on DE will be tighter. This work

\* benidav@post.bgu.ac.il

† vasak@fias.uni-frankfurt.de

‡ struckmeier@fias.uni-frankfurt.de

§ stoecker@fias.uni-frankfurt.de

Typical System	Quantity	Value related Dark Energy	Curvature Scalar $\mathcal{K} = R_{\alpha\beta\mu\nu}R^{\alpha\beta\mu\nu}$
Point mass	$r_V/r$	$r_V^3 = 3GM/\Lambda c^2$	$\frac{2}{3}\Lambda^2 [1 + 72(r_V/r)^6]$
Binary system	$\kappa = (T_{\text{kep}}/T_\Lambda)^2$	$T_\Lambda \approx 35 \text{ Gy}$	$\left(\frac{GM}{c^2 r^3}\right)^2 \left(48 + \frac{2}{3}\kappa^2\right)$
Spherical Density	$\Delta_c = \rho_s/\rho_\Lambda$	$\rho_\Lambda^{Pl} = (5.78 \pm 0.11) \times 10^{-27} \text{ kg/m}^3$	$\frac{256}{3} \left(\frac{G\pi}{c^2}\right)^2 (1 + \Delta_c^2)$

TABLE I. The table shows different representations of the cosmological constant in different systems. For point mass the critical radius separates distances of the Newtonian force domination vs. distances with  $\Lambda$  repulsion force domination. Correspondingly, in binary motion that critical value is the orbital period of the motion vs.  $T_\Lambda$ . In a spherical density model, the scaling density  $\rho_s$  is critical value vs. the cosmological constant related one  $\rho_\Lambda$ . The related curvature scalar invariant  $\mathcal{K} = R_{\alpha\beta\mu\nu}R^{\alpha\beta\mu\nu}$  is also presented.

extends Ref. [78] from binary motion to a spherical mass density in general, and galaxies in particular. Moreover, while Ref. [78] correlates the curvature of the system with the frequency of the binary motion (and therefore to the upper bound on DE), this work correlates curvature with the mass density.

The structure of the paper is as follows: Section II summarizes the criteria for DE domination. Section III develops the theoretical framework for a spherical density model with DE. Section IV describes the data set and the method for constraining the DE by an upper bound. Section V compares the results with other systems. Section VI provides an outlook on further research and discusses the efficiency of testing DE models.

## II. EQUIVALENT DARK ENERGY DOMINATION CONDITIONS

There are few criteria to test the dominance of DE. In principle, all of these criteria use the same equilibrium in which the outward-directed influence of  $\Lambda$  is balanced by the inward-directed gravitational attraction as reference.

- **Point Mass:** The radius of the zero acceleration surface, where the total force in Eq. (1) is zero, reads:

$$r_V = \sqrt[3]{\frac{3GM}{\Lambda c^2}}. \quad (2)$$

For  $r < r_V$  the Newtonian attraction governs, and for  $r > r_V$  the DE repulsion force dominates the acceleration. These conditions play a role in the analysis of galaxy clusters in the local Universe [63, 80–82].

- **Binary Motion:** In the context of binary motion it is then possible to quantify the impact of  $\Lambda$  versus the Newtonian force via the ratio between the two terms on the right-hand side of Eq. (1):

$$\kappa := (T_{\text{Kep}}/T_\Lambda)^2, \quad (3)$$

where the Keplerian period is given by

$$T_{\text{Kep}} = 2\pi\sqrt{\frac{r^3}{GM}}. \quad (4)$$

The critical period associated with the cosmological constant is, on the other hand,

$$T_\Lambda = \frac{2\pi}{c}\sqrt{\frac{3}{\Lambda}}. \quad (5)$$

For  $T_K < T_\Lambda$  the Newtonian force prevails, whereas for  $T_K > T_\Lambda$  the repulsion caused by the cosmological constant dominates. This condition has been found in [76] where it was shown that, for Milky Way and Andromeda as a binary system,  $\kappa$  has a non-negligible effect<sup>1</sup>. This implies a dominant Newtonian force for this system. In fact, Ref. [78] compares various binary systems with regard to the upper bound on  $\Lambda$  and its correlation with  $\kappa$ . From the value of the cosmological constant derived by the Planck collaboration,  $T_\Lambda$  is [8]:

$$T_\Lambda^{\text{Planck}} = 36.75 \pm 0.32 \text{ Gy}, \quad (6)$$

while the value from the SH0ES data is [83]:

$$T_\Lambda^{\text{SH0ES}} = 34.13 \pm 0.66 \text{ Gy}. \quad (7)$$

The densities have a  $3\sigma$  difference which is related to the Hubble tension [84, 85].

- **Spherical Density:** For a rotating spherical density, the relation between the periods can be replaced by a relation between the density of the structure and the critical density due to dark energy. With the scaling density  $\rho_s$  and the scaling period  $T_s$  at that point, the frequency of the spherical orbit can be expressed as [86]:

$$\left(\frac{2\pi}{T_s}\right)^2 = \frac{4}{3}\pi G\rho_s. \quad (8)$$

Half of the ratio between the attractive Newtonian potential at the critical radius  $r_s$  and the dark energy repulsion gives the dimensionless, so-called overdensity parameter.

$$\Delta_c := \frac{\rho_s}{\rho_\Lambda} = \frac{1}{2} \frac{GM(r_s)/r_s^3}{\Lambda c^2/3}. \quad (9)$$

<sup>1</sup> Ref. [76] defines the  $T_\Lambda$  without the 1/3 factor. Here, for the complementary comparison, we define the  $T_\Lambda$  with the 1/3 factor and the value becomes comparable to the age of the Universe.

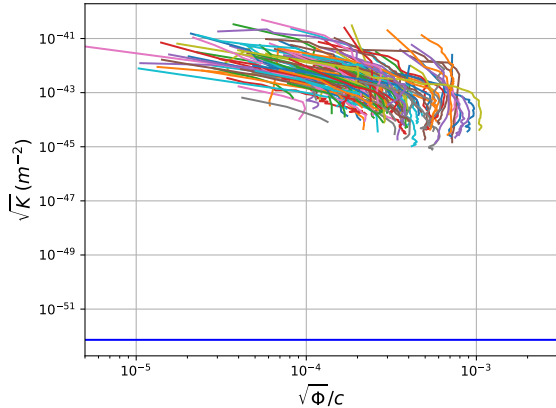


FIG. 1. *The normalized potential  $\sqrt{\Phi}/c$  vs. the scalar-curvature  $\sqrt{K}$  of galaxies extracted directly from the SPARC dataset via the measured circular velocities. The galaxy curves are parameterized by the distance from its center. The Planck value of the cosmological constant is presented in blue line.*

$r_s$  is the scaling radius where the dark matter density model changes its behavior,  $\rho_s$  is the average density within the critical radius,

$$\rho_s := \frac{\int_0^{r_s} \rho(r) d^3r}{\int_0^{r_s} d^3r} =: \frac{M(r_s)}{\frac{4\pi}{3} r_s^3}, \quad (10)$$

and  $\rho_\Lambda \equiv \Lambda c^2/8\pi G$  is the energy density that is associated with DE.

To determine  $\rho_\Lambda$ , there are two choices for  $\Lambda$  to be inserted into Eq. (5). With a constant density, for  $\rho_s > 2\rho_\Lambda$  the Newtonian force governs and for  $\rho_s < 2\rho_\Lambda$  the repulsion force of  $\Lambda$  governs. From the value of the cosmological constant derived by the Planck collaboration,  $\rho_\Lambda$  is [8]:

$$\rho_\Lambda^{\text{Planck}} = (5.78 \pm 0.11) \times 10^{-27} \text{ kg/m}^2, \quad (11)$$

while the value from the SH0ES data is [83]:

$$\rho_\Lambda^{\text{SH0ES}} = (6.75 \pm 0.26) \times 10^{-27} \text{ kg/m}^2. \quad (12)$$

Of course, the analysis suggested here depends on the system under consideration. Table (I) summarizes three different approaches for quantifying the domination of dark energy in point-mass binaries, extended binary systems, and spherical densities. This research focuses on constraining DE from galaxies, and therefore uses the latter approach.

### III. FLAT ROTATION CURVES WITH DARK ENERGY

#### A. Schwarzschild-de Sitter Spacetime

The line element  $ds^2$  for the de Sitter-Schwarzschild (DSS) spacetime reads:

$$ds^2 = -(1 - \Phi(r)) dt^2 + \frac{dr^2}{1 - \Phi(r)} + r^2 [d\theta^2 + \sin^2 \theta d\phi^2], \quad (13)$$

in which  $\theta$  and  $\phi$  are the usual spherical angles. The potential reads:

$$\Phi(r) = \frac{2GM(r)}{c^2 r} + \frac{1}{3} \Lambda r^2, \quad (14)$$

where  $M(r)$  is the integrated density up to the radius  $r$ . The term captures the gravitational-potential and dark-energy contributions. It is thus a de Sitter-Schwarzschild metric which reduces to the Schwarzschild metric in the limit of  $\Lambda = 0$ . For tracking the impact of the cosmological constant in different systems, we use the gauge-invariant curvature of spacetime, i.e., the Kretschmann scalar:

$$\mathcal{K} \equiv R^\lambda_{\alpha\beta\gamma} R_\lambda^{\alpha\beta\gamma}, \quad (15)$$

in which  $R^\lambda_{\alpha\beta\gamma}$  is the Riemann tensor. For a spherical density model in the de Sitter-Schwarzschild metric, the Kretschmann scalar at the distance  $r$  from the center reads:

$$\mathcal{K} = 48 \left( \frac{GM(r)}{c^2 r^3} \right)^2 + \frac{2}{3} \Lambda^2. \quad (16)$$

For a spherical structure with a scaling density  $\rho_s$ , the potential and the curvature scalar can be written as:

$$\Phi(r_s) = \frac{8\pi G \rho_s}{3c^2} (1 + \Delta_c^{-1}) r_s^2, \quad (17a)$$

$$\mathcal{K} = \frac{256}{3} \left( \frac{G\pi}{c^2} \right)^2 (1 + \Delta_c^{-2}), \quad (17b)$$

with the inverse overdensity quantifying the relative impact of  $\Lambda$  versus the matter density.

The observational data for the rotation curves considered in this work are taken from the catalog Spitzer Photometry & Accurate Rotation Curves (SPARC)<sup>2</sup> sample [13] which contains 175 disk galaxies. As a rough estimation for the potential and the curvature, we use combinations with  $v(r)$  and  $r$  (assuming  $v_i^2 = GM(r_i)/r_i$ ):

$$\Phi = 2 \left( \frac{v_i}{c} \right)^2 + \frac{1}{3} \Lambda r_i^2, \quad \mathcal{K} = 48 \left( \frac{v_i}{c r_i} \right)^2 + \frac{2}{3} \Lambda^2, \quad (18)$$

<sup>2</sup> <http://astroweb.cwru.edu/SPARC/>

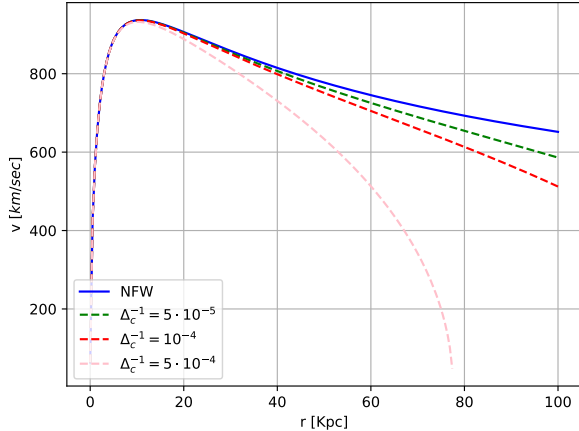


FIG. 2. The circular velocity of galaxy for the NFW profile without and with different values of DE. For larger  $\Lambda$  the maximal velocity is reduced and setting the boundary for the galaxy flat rotation curves.

where  $v_i = v(r_i)$  and  $r_i$  are the individual velocities and radii from the data.

Fig. (1) shows the potential vs. the curvature scalar for the SPARC dataset. We see that there is a few orders difference between the standard curvature of the galaxy and the curvature from the cosmological constant (solid line in blue), which indicates that we may only get an upper bound, but not a detection for DE. However, it seems that with a better fit we may reduce the upper bound and, as we shall see, push the upper bound surprisingly closer to the actual value.

### B. Virial radius

Three different characteristic phases during the evolution can then be identified:

- **The turnaround radius:** This is, as discussed, the distance from the center where the sphere breaks away from the general expansion and reaches a maximum radius.
- **The collapse radius:** The surface where the sphere collapses towards a central singularity while the densities of the matter fields would formally go to infinity. Practically, the pressure and dissipation intervene well before this singularity is reached and convert the kinetic energy of the collapse into random motions.
- **The virialization radius:** It specifies where the dynamical equilibrium is reached and the system becomes stationary. Then, the radius of the system and the energy of the different components are constant. The virial radius of a gravitationally bound

astrophysical system is the radius within which the virial theorem applies. It is defined as the radius at which the density is equal to the critical density  $\rho_c$  of the universe at the redshift of the system, multiplied by an overdensity constant. The overdensity constant depends on the cosmological background model. For the Einstein-de Sitter model the overdensity is [87]:

$$\Delta_c \approx 18\pi^2 \approx 178.$$

The exact value of  $\Delta_c$  depends on the background cosmology. For the  $\Lambda$  Cold Dark Matter model, the overdensity parameter  $\Delta_c \approx 100$  at a redshift of zero. Nevertheless, it is typically assumed that  $\Delta_c = 200$  for the purpose of using a common definition:  $r_{200}$  for the virial radius and  $M_{200}$  for the virial mass. Similarly,

$$x_{200} \equiv r_{200}/r_s, \quad v_{200} \equiv 10 x_{200} r_s H_0,$$

where  $x_{200}$  is the concentration parameter,  $v_{200}$  the velocity at  $r_{200}$  and  $H_0$  is the Hubble parameter. In our research, we show that  $\Delta_c$  can be calibrated by the data.

### C. Spherical Dark Matter models

The equations of motion of a massive particle in the gravitational field described by the general spherically symmetric metric can be obtained from the geodesic equation. Ref. [75] shows that the circular velocity  $v_{\text{hal}}$  of the halo density is given by

$$v_{\text{hal}}^2(r) = \frac{1}{1 - \Phi(r)} \left[ \frac{GM(r)}{r} - \frac{1}{3}\Lambda c^2 r^2 \right]. \quad (19)$$

For  $\Phi(r) \ll 1$  we recover the Newtonian approximation, where  $\Lambda$  acts as a linear repulsion force. For spherical model of mass  $M(r)$  the Newtonian contribution for the velocity is  $v_N^2(r) = GM(r)/r$ . DE acts as a repulsion force and gives a maximal value for a radius where  $v_{\text{hal}} = 0$ .

For two-power density models, the luminosity density of many elliptical galaxies can be approximated by a power law in radius at both the largest and smallest observable radii, with a smooth transition between these power laws at intermediate radii. Numerical simulations of the clustering of dark-matter particles suggest that the mass density within a dark halo has a similar structure. We test two different models, the NFW and the Hernquist model [88]:

$$\bar{\rho}(x) = \frac{\rho(x)}{\rho_s} = \begin{cases} \left( x(1+x)^2 \right)^{-1} & \text{NFW,} \\ \left( x(1+x)^3 \right)^{-1} & \text{Hernquist,} \end{cases} \quad (20)$$

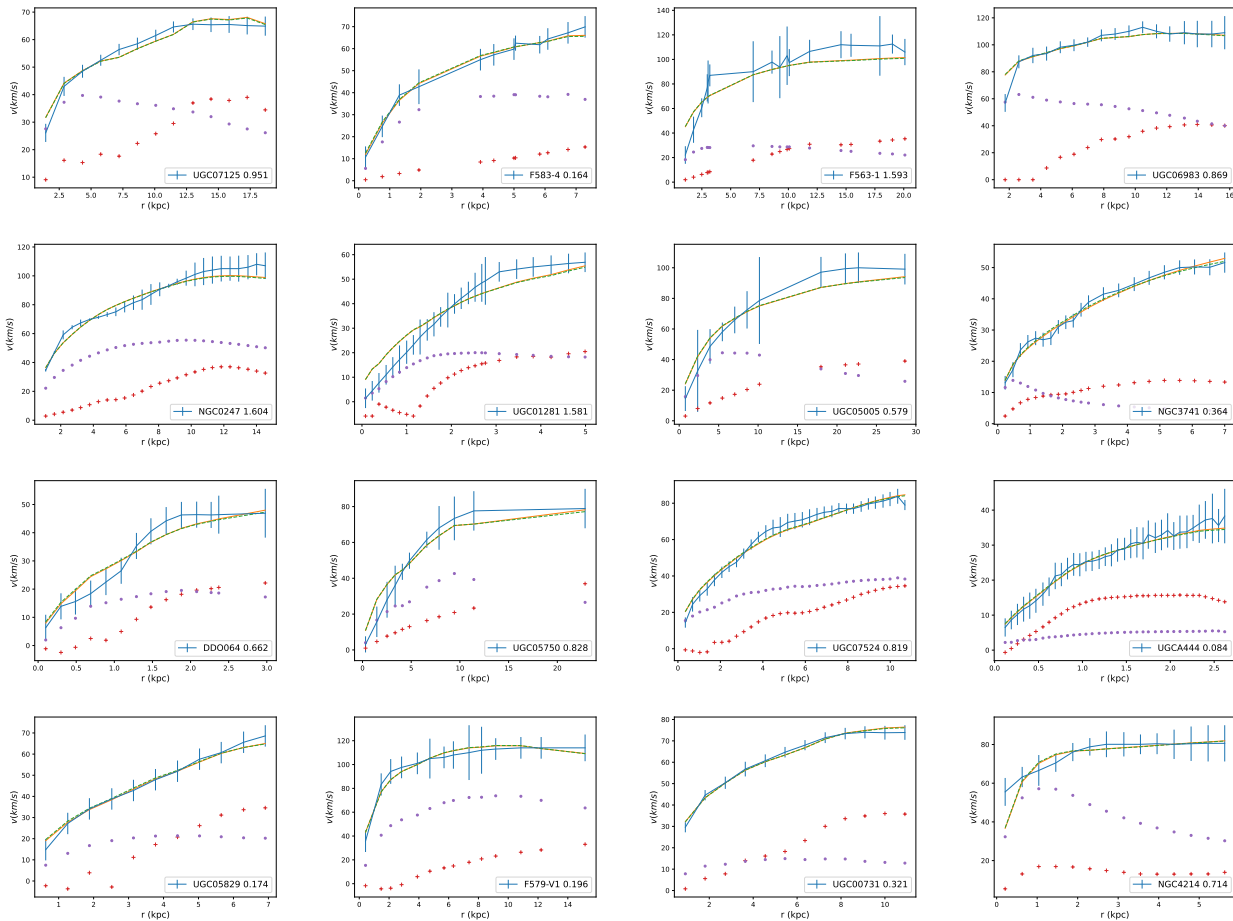


FIG. 3. Examples for fits of different galaxies with the NFW profile without  $\Lambda$  (smooth orange) for the NFW model. The observed velocity  $v_{\text{obs}}$  with the corresponding errors are in blue, while the fit is in orange. The gas velocity is noted with “+”, the disk velocity is noted by “.”. The reduced  $\chi^2$  is also presented. In general, the models are sufficiently flexible to reproduce the observational data to good accuracy.

where  $x = r/r_s$  is the scaled radius. The corresponding mass density for these models gives the following:

$$\bar{M}(x) = \frac{M(x)}{16\pi\rho_s r_s^3} = \begin{cases} \ln(1+x) - \frac{x}{1+x} & \text{NFW,} \\ \frac{x^2}{2(1+x^2)} & \text{Hernquist.} \end{cases} \quad (21)$$

To find the velocity for different models, we insert the mass vs.  $x$  model in Eq. (19). Fig. (2) shows schematically the scaled flat rotation curves of a typical galaxy for the NFW profile without and with two different values of DE. For larger values of  $\Lambda$  the maximal possible velocity decreases. It is possible to normalize the halo velocity term, Eq. (19), by using the overdensity  $\Delta_c$ , as:

$$v_{\text{hal}}^2(x) = \frac{v_s^2}{1 - \Phi(x)} \left[ \frac{\bar{M}(x)}{x} - \frac{2}{3} \Delta_c^{-1} x^2 \right]. \quad (22)$$

with  $v_s := 2r_s\sqrt{\pi G\rho_s}$ . The fit for the flat rotation curves give an upper bound for the  $\Delta_c^{-1}$  parameter and therefore an upper bound for  $\rho_\Lambda$ .

## IV. BOUNDS ON $\Lambda$

### A. Analysis methodology

We test the upper bound for  $\Lambda$  from the SPARC dataset [14–31]. The SPARC database includes 175 late-type galaxies with high-quality rotation curves detected via near-infrared Spitzer photometry. The measurements allow tracing the rotation velocity out to large radii, providing strong constraints on the dark matter halo profiles. The mass models for the stellar disk are built by numerically solving the Poisson equation for the observed surface brightness profile. The derived gravitational potentials of the baryonic components are represented by the circular velocities of the test particles, tabulated as  $v_{\text{disk}}$ ,  $v_{\text{bul}}$ , and  $v_{\text{gas}}$  corresponding to the contributions of the stellar disk, bulge, and gas, respectively.

The predicted circular velocity  $v_{\text{pred}}$  in the galactic plane is broken down into contributions from the gas,



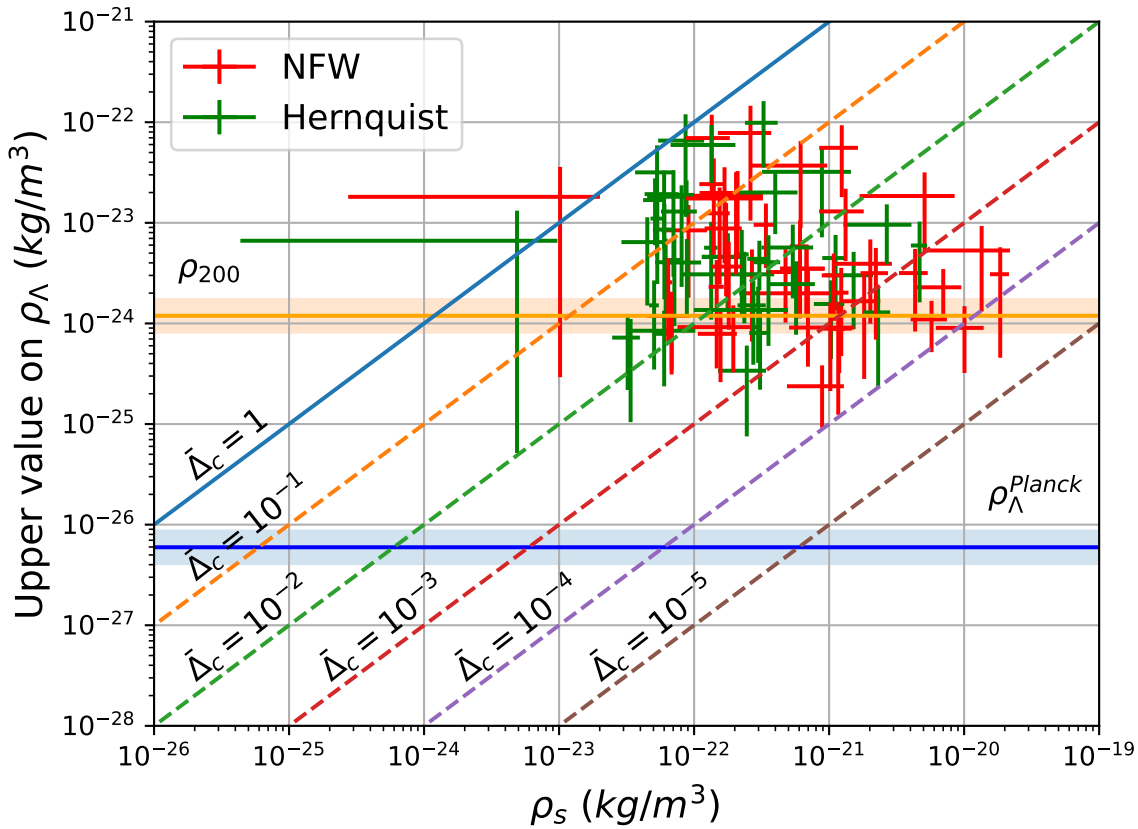


FIG. 4. The upper bounds on  $\Lambda$  vs. the corresponding scaling density for different galaxies for the NFW (red) and the Hernquist models (green) with a cosmological constant presence. The lines above corresponds to different values of  $\bar{\Delta}_c^{-1} = \rho_{(<\Lambda)} / \rho_s$ . The area above the dashed blue line,  $\bar{\Delta}_c^{-1} > 1$ , is a “forbidden area” where the DE energy density is larger then the scaling density of the galaxy. The galaxies fit give wide range of  $\bar{\Delta}_c^{-1}$  in between 1 and  $10^{-4}$ . The fitted upper bound (defined by  $1\sigma$  deviation for the mean posterior value) sits around  $\rho_{200}$ .

disk and dark matter halo:

$$v_{\text{pred}}^2 = v_{\text{hal}}^2 + v_{\text{gas}}^2 + \Upsilon_{\text{disk}} v_{\text{disk}}^2. \quad (23)$$

The contributions  $v_{\text{gas}}$ ,  $v_{\text{disk}}$  (and  $v_{\text{bul}}$ ) are deduced from the HI gas density and the light profiles, respectively, and provided by SPARC. The  $\Upsilon_{\text{disk}}$  is the stellar mass-to-light ratio for the disk (bulge) and it is equivalent to the mass  $M_D$  of the disk divided by the luminosity  $L_D$  of the disk. We choose galaxies without bulge contribution to reduce the degeneracy with other degrees of freedom to the fit. The  $v_{\text{hal}}$  is the circular velocity from Eq. (19).

We use Bayesian analysis to find the best parameters,  $r_s, \rho_s$  implicitly through  $v_s$ , and  $\Lambda$ , for each galaxy vs. the observational data. We assume that the errors of the observed rotation curve data follow a Gaussian distribution, so that we can build the  $\chi^2$  defined as:

$$\chi^2 = \left( \frac{v_{\text{obs}} - v_{\text{pred}}(r_s, v_s, \Upsilon_{\text{disk}}, \bar{\Delta}_c^{-1})}{\sigma_v} \right)^2 \quad (24)$$

where  $v_{\text{obs}}$  is the observed velocity with the error  $\sigma_v$  while the prediction is  $v_{\text{pred}}$ , Eq. (23). To give the upper

value of  $\Lambda$  as a repulsion force, we test the zero-point surface where  $v = 0$  or  $\Delta_c = 1$ . For the likelihood maximization, we used an affine-invariant MCMC nested sampler, as it is implemented within the open-source package `Polychord` [89] with the `GetDist` package [90], to present the results.

We use the following flat priors:  $v_s \in [0, 200]$  km/sec,  $r_s \in [0, 50]$  Kpc,  $\Upsilon_D \in [0.2, 1.5]$ . For the cosmological constant we used the range:  $\bar{\Delta}_c^{-1} \in [0, \bar{\Delta}_c^{\text{max}}]$ , with  $\Lambda_{\text{max}}$  derived from the maximum value of  $\bar{\Delta}_c^{-1}$ . For a given  $r_s$ , we calculate the corresponding  $x_i = r_i/r_s$  of the dataset. We calculate for the given  $x_i$  set the solutions for  $\Lambda_{\text{max}}$  with  $v = 0$  with the upper value of the prior, giving the maxima of the corresponding set:  $\bar{\Delta}_c^{\text{max}} = \max_i M(x_i)/x_i^3$ . The selection criteria for good fit models for the MCMC is:

$$\chi_{\text{red}}^2 = \chi^2 / (N - d + 1) \leq 1.7, \quad (25)$$

where  $\chi_{\text{red}}^2$  is the reduced  $\chi^2$  normalized by the number of degrees of freedom - the number of points for an individual galaxy  $N$  minus the number of parameters  $d = 4$

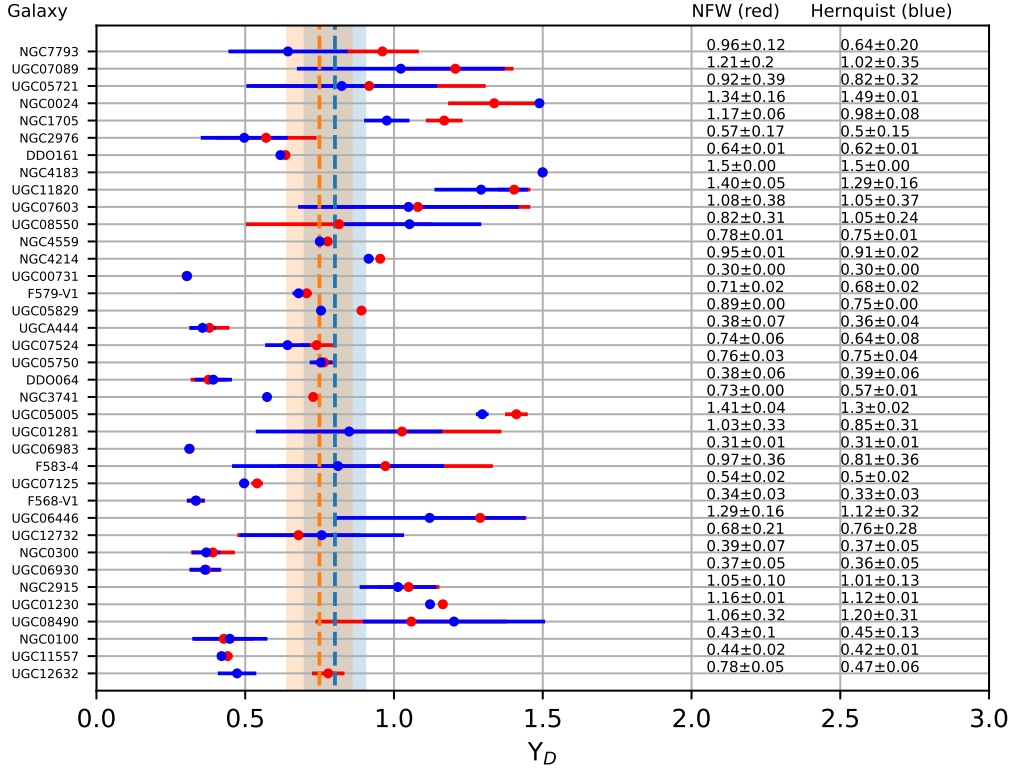


FIG. 5. The final fitted values of  $\Upsilon_D$  for the good fit galaxies for the NFW density profile (blue) and for the Hernquist density profile (red) with  $1\sigma$ . The average value of the mass to light ratio is  $\bar{\Upsilon}_D = 0.79 \pm 0.11$  for the NFW model and  $\bar{\Upsilon}_D = 0.74 \pm 0.10$  for the Hernquist model.

plus one. For this selection criteria we are left with  $\sim 50$  appropriate galaxies.

## B. Results

Fig. (3) shows examples of good fit for the NFW model. The observed velocity with the corresponding errors is colored blue, whereas the fit is colored orange. The velocity of the gas is observed with “+”, the disk velocity is noted by “.”. The reduced  $\chi^2_{\text{red}}$  is also presented. The fit including  $\Lambda$  (orange dashed lines) is similar to the fit for the purely Newtonian potential (coupled to the dark-matter model). This implies only a minor impact of  $\Lambda$ , and the fit yields an upper bound for  $\Lambda$ . We define this upper bound as the  $1\sigma$  confidence bound around the mean. Fig. (4) shows the upper bound on  $\Lambda$  vs. the corresponding scaling densities of different galaxies for the NFW (red) and the Hernquist models (green).

The lines correspond to  $\bar{\Delta}_c^{-1} := \rho_{(<\Lambda)}/\rho_s$ . The area above the dashed blue line,  $\bar{\Delta}_c^{-1} > 1$ , is the “forbidden area” where the repulsion force of  $\Lambda$  is so strong that the galaxy would not exist anymore. The possibility of a virialized close galaxy from the fit exists with  $1\sigma$  probability.

Besides one outlier, a galaxy where the posterior is with a huge error bar, all galaxies obey this principle and have  $\bar{\Delta}_c^{-1} \ll 1$  in the range  $10^{-1}$  to  $10^{-4}$ .

We define the upper bound on  $\rho_\Lambda$  as the mean+ $1\sigma$  value. Therefore, the upper bound of  $\rho_\Lambda$  is in the range  $10^{-22}$  kg/m<sup>3</sup> to  $10^{-25}$  kg/m<sup>3</sup> for the lowest cases. In order to compare results from different galaxies, we also display the value of  $\rho_\Lambda$  by Planck together with the  $\rho_{200}$  value. According to the virialization of spherical density over cosmological background,  $\rho_{200}$  is the corresponding value of the density at the outskirts of the galaxies. We expect that the upper bound on  $\Lambda$  will be reduced further once more data close to these points are available. Since the measurements to date are only around the  $r_s$  region, the upper bound on  $\Lambda$  approaches  $\rho_{200}$  only for a subset of the sample.

Fig. (4) shows that albeit the NFW model predicts slightly higher values, the results are robust for different models of dark matter. Since the NFW model is more cuspy in the center and the Hernquist shallower, the former model predicts higher values. Fig. (5) shows the final fitted values of  $\Upsilon_D$  for the good-fit galaxies for the NFW density profile (blue) and for the Hernquist density profile (red). The average value of the mass to

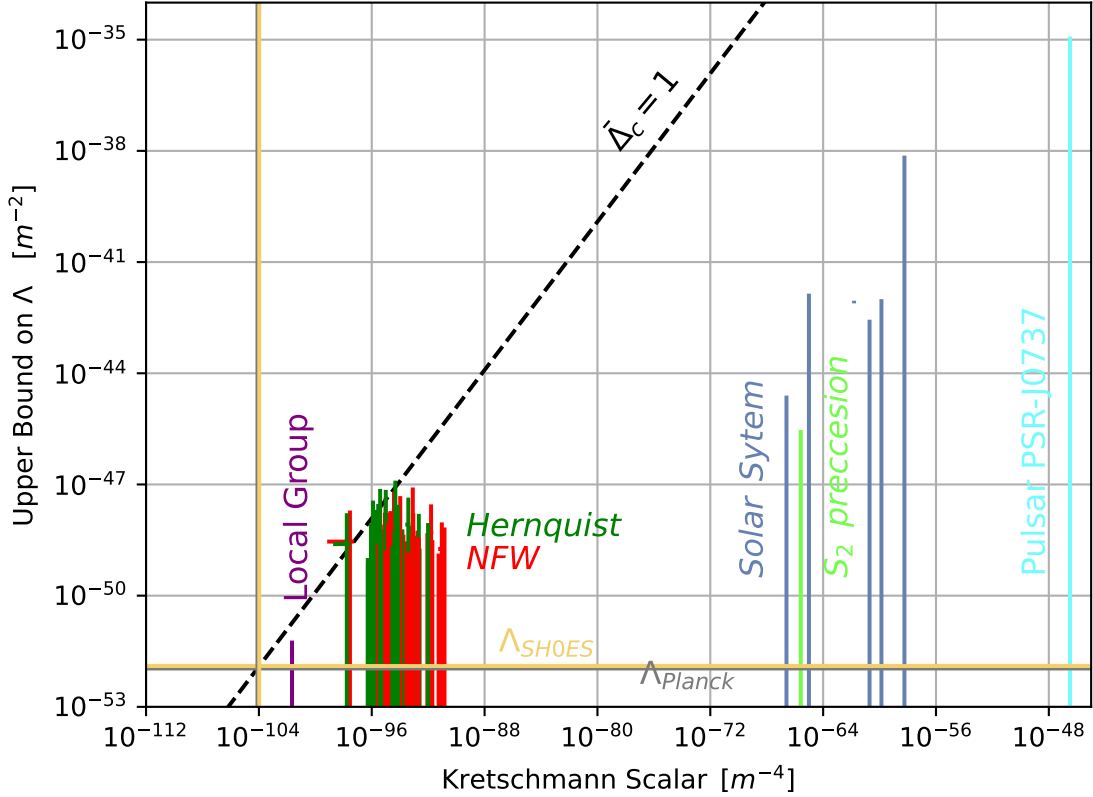


FIG. 6. Comparison between bounds on the cosmological constant for different systems versus the curvature scalar for these systems: planets in the solar system (dark blue), S2 star around Sgr A\* (green), double pulsar PSR J0737-3039A/B (azure), Local Group (purple) with the new fit discussed in [78]. Each upper bound is the  $5\sigma$  upper bound on  $\Lambda$ . For comparison, we put the estimated values of the cosmological constant from [8] (grey) and SHOES [83], (yellow). For longer periods in binary motions or lower spherical densities in galaxies, the upper bound on  $\Lambda$  decreases and getting close to the one measured from Cosmology.

light ratio is  $\tilde{\Upsilon}_D = 0.79 \pm 0.11$  for the NFW model, and  $\tilde{\Upsilon}_D = 0.74 \pm 0.10$  for the Hernquist model. In the literature,  $\tilde{\Upsilon}$  reads  $\sim 0.7$  which is compatible with our posterior distribution.

### C. Degeneracy in DE models

We would like to point out the limitation of analyzing galactic flat rotation curves as advocated here to derive further information on DE models. The main obstacle to constraining DE models is the degeneracy between any additional parameters and  $\Lambda$ . Take, as an example, Ref. [12] that generalizes the potential in Eq. (14) by a variable Equation of State (EoS):

$$\phi = \frac{2GM}{rc^2} + \left( \sqrt{\frac{6}{\Lambda}} \frac{1}{r} \right)^{3w+1}, \quad (26)$$

where  $w$  is the EoS parameter. For  $w = -1$  the potential in Fig. 5 of Ref. [12] shows that the best fit of  $w$  is degenerate with the best fit of the radius,  $r_0 = \sqrt{6/\Lambda}$ . Hence, constraining both parameters,  $w$  and  $r_0$ , at once is not possible, only a relation between these two parameters can be derived. Another point in the constraints from [12] is the parameter setting. Ref. [12] sets a prior on  $r_0$  rather than on  $\Lambda$ . In our approach we set a prior on  $\Lambda$  such that the possibility for  $\Lambda = 0$  is retained that recovers the Newtonian potential. However, because of the relation  $r_0 \sim 1/\Lambda$ , setting it prior to  $r_0$  restricts that freedom.

Another example for a parameter degeneracy is the introduction of a Yukawa potential correction:

$$\phi = \frac{2GM}{rc^2} (1 + \beta e^{-m_g r}), \quad (27)$$

as proposed in Ref. [91–95], where  $\beta$  is the Yukawa strength and  $m_g$  is the graviton mass. For vanishing  $\beta$  the Yukawa interaction is reduced to the Newtonian one.



For vanishing  $m_g$  the Newtonian constant is modified to  $G(1 + \beta)$ . Such a correction arises whenever the force is mediated by a scalar particle of mass  $m_g$ . Therefore, testing gravity is equivalent to testing the existence of a fifth force of scalar nature. As Ref. [55] shows,  $\beta$  and  $m_g$  are degenerate via  $m_g = b|\beta|^{-c}$  with constants  $b$  and  $c$ . In both cases, it is not possible to constrain the parameters, unless the degeneracy is broken by an additional condition on any of the parameters.

## V. CONSISTENCY WITH OTHER PROBES

The bounds discussed in this paper are compatible with the recent result of [76–78] even though they are based on different datasets. Fig. (6) plots the upper bounds on  $\Lambda$ , derived from various astrophysical systems, vs. the corresponding curvature around those systems. Some of those systems are binary systems, while the systems discussed here are spherical densities.

For binary systems their orbital frequency is the parameter that quantifies the curvature over DE. Eq. (16) can be formulated as:

$$\mathcal{K} = 48 \left( \frac{\omega_{\text{Kep}}}{c} \right)^4 + \frac{2}{3} \Lambda^2, \quad (28)$$

where the orbital frequency of the system  $\omega_{\text{Kep}}$  is related to the curvature. The binary systems that Ref. [78] discusses includes the Solar System planets, the S2 star around the galactic center, the Double Pulsar PSR-J0737, and the binary motion of the Milky Way and M31 galaxies. Albeit the measurements of the Double Pulsar is much more accurate than the measurements of the Local Group, the constraints on  $\Lambda$  from the Local Group are the tightest ones, since for the binary motion the curvature is closer to the ambient one furnished by  $\Lambda$ . In particular, the orbital frequency of the Local Group is much smaller than the orbital frequency of the Double Pulsar, giving the smallest deviation from the  $\Lambda^2$  term in Eq. (28).

Probing DE on spherical structures, on the other hand, is based on exploring its ambient energy density pulling the structure apart against the Newtonian force. Ref. [96] compares different spherical systems and shows the impact of DE in cases where  $\rho_s$  and  $\rho_\Lambda$  are similar. In our derivation, Eq. (17b) correlates the matter density to the curvature and shows too that for  $\rho_s \sim \rho_\Lambda$  the curvature changes due to the interplay between the dark matter and the DE densities. The spherical system in question are in particular the following:

- **Galaxies from the SPARC dataset:** The galactic (SPARC) data are in the focus of this paper where we select galaxies according to suitability for the analysis of DE upper bounds. By assuming the model of the dark matter, it is possible to probe the potential on top of that density. We assume the NFW and the Hernquist models. The overall estimate for the upper bound is

about  $\Lambda < 1.5 \times 10^{-48} \text{ m}^{-2}$ , with some particular galaxies restricting the upper bound on  $\Lambda$  even stronger.

- **Milky Way:** Milky Way is a barred spiral galaxy, about  $10^3$  light-years thick at the spiral arms (more at the bulge) [97] with specific aspects that need to be taken into account in this analysis. Ref. [12] reports on Dark Energy constraint on the Milky Way while assuming NFW for the dark matter model and setting the potential as in Eq. (26). That leads to the constraint  $r_0/\sqrt{6/\Lambda} < 0.1$  which gives  $\Lambda < 1.5 \times 10^{-47} \text{ m}^{-2}$ . The virialized radius of the Milky Way is about  $r_{\text{vir}} \sim 200$  Kpc while the measurements of Ref. [12] cover the range up to about 100 Kpc. With future measurements closer to the  $r_{\text{vir}}$  the upper bounds will be improved.
- **Laniakea Supercluster:** The Laniakea Supercluster is home to Milky Way and approximately  $10^5$  other nearby galaxies. It will disperse rather than continue to maintain itself as an overdensity relative to surrounding areas. The overall density of this supercluster is close to  $\rho_\Lambda$  [98, 99]. This gives a possible system to test the DE impact depending on the model of the cluster, for instance [100].

## VI. SUMMARY AND DISCUSSION

This work applies the observational data from the SPARC dataset to constrain Dark Energy (DE) in a spherically symmetric surroundings of galactic dark-matter halos. We use the Navarro-Frenk-White (NFW) and Hernquist models to identify the most suitable galaxies for these models. The DE acts as a repulsive force on galactic dark-matter halos agglomerated via Newtonian attraction. We show that albeit the DE scale is related to a length scale, the upper bound on  $\Lambda$  is correlated to the density of the surroundings and the efficiency of the measurements.

The fits of the overdensities,  $\bar{\Delta}_c^{-1}$ , for selected galaxies give a wide range of values between 1 and  $10^{-4}$ . The fitted upper bound (defined by  $1\sigma$  deviation for the mean posterior value) sits around  $\rho_{200}$  giving an upper bound on DE around  $\rho_{(<\Lambda)} \sim 10^{-25} \text{ kg/m}^3$ , only two orders of magnitude larger than that measured in cosmological studies by the Planck collaboration.

DE acts in different ways in different systems. For point masses, the critical radius separates distances of the Newtonian force domination vs. distances where  $\Lambda$  repulsion dominates. Consequently, in binary motion, that critical value is the orbital period of the motion vs.  $T_\Lambda$ . In a spherical density model, on the other hand, the scaling density  $\rho_s$  is the critical quantity to compare with the ambient DE density  $\rho_\Lambda \sim 10^{-27} \text{ kg/m}^3$  given by the cosmological constant. We discuss different models of DE and modified gravity, and we also address degeneracies with DE model parameters.

For improving the upper bound, the data in future measurements must be closer to the outskirts of the galaxies, where the dark-matter densities are closer to  $\rho_\Lambda$  and the effect of DE is more pronounced. The **James Webb Space Telescope** post to measure the outskirts of the Milky Way and other galaxies. In that case, we claim that the upper bound of  $\Lambda$  could possibly be detected as an additional slope in the velocity rotation curve (see Fig. (2)), and we expect that the value of the fitted  $\rho_{(<\Lambda)}$  will be closer to  $\rho_\Lambda$  than to  $\rho_{200}$ .

## ACKNOWLEDGMENTS

*DB and DV thank the Carl-Wilhelm Fueck Stiftung for support. DB is also grateful for the support from the Margarethe und Herbert Puschmann Stiftung and the European COST action CA21136.*

- 
- [1] P. J. E. Peebles and B. Ratra, *Rev. Mod. Phys.* **75**, 559 (2003), [arXiv:astro-ph/0207347](#).
- [2] S. Perlmutter *et al.* (Supernova Cosmology Project), *Astrophys. J.* **517**, 565 (1999), [arXiv:astro-ph/9812133](#).
- [3] D. M. Scolnic *et al.* (Pan-STARRS1), *Astrophys. J.* **859**, 101 (2018), [arXiv:1710.00845 \[astro-ph.CO\]](#).
- [4] G. E. Addison, G. Hinshaw, and M. Halpern, *Mon. Not. Roy. Astron. Soc.* **436**, 1674 (2013), [arXiv:1304.6984 \[astro-ph.CO\]](#).
- [5] E. Aubourg *et al.*, *Phys. Rev. D* **92**, 123516 (2015), [arXiv:1411.1074 \[astro-ph.CO\]](#).
- [6] A. J. Cuesta, L. Verde, A. Riess, and R. Jimenez, *Mon. Not. Roy. Astron. Soc.* **448**, 3463 (2015), [arXiv:1411.1094 \[astro-ph.CO\]](#).
- [7] A. Cuceu, J. Farr, P. Lemos, and A. Font-Ribera, *JCAP* **10**, 044 (2019), [arXiv:1906.11628 \[astro-ph.CO\]](#).
- [8] N. Aghanim *et al.* (Planck), *Astron. Astrophys.* **641**, A6 (2020), [Erratum: *Astron. Astrophys.* 652, C4 (2021)], [arXiv:1807.06209 \[astro-ph.CO\]](#).
- [9] V. Trimble, *Ann. Rev. Astron. Astrophys.* **25**, 425 (1987).
- [10] J. Calcino, J. Garcia-Bellido, and T. M. Davis, *Mon. Not. Roy. Astron. Soc.* **479**, 2889 (2018), [arXiv:1803.09205 \[astro-ph.CO\]](#).
- [11] N. Gomes-Oliveira *et al.*, (2023), [arXiv:2310.13839 \[astro-ph.GA\]](#).
- [12] R. Zhang and Z. Zhang, *JCAP* **06**, 031 (2023), [arXiv:2303.14047 \[gr-qc\]](#).
- [13] F. Lelli, S. S. McGaugh, and J. M. Schombert, *Astron. J.* **152**, 157 (2016), [arXiv:1606.09251 \[astro-ph.GA\]](#).
- [14] F. Lelli, S. S. McGaugh, J. M. Schombert, and M. S. Pawlowski, *Astrophys. J. Lett.* **827**, L19 (2016), [arXiv:1607.02145 \[astro-ph.GA\]](#).
- [15] S. McGaugh, F. Lelli, and J. Schombert, *Phys. Rev. Lett.* **117**, 201101 (2016), [arXiv:1609.05917 \[astro-ph.GA\]](#).
- [16] F. Lelli, S. S. McGaugh, and J. M. Schombert, "Astrophys. J. Lett." **816**, L14 (2016), [arXiv:1512.04543 \[astro-ph.GA\]](#).
- [17] F. Lelli, S. S. McGaugh, J. M. Schombert, and M. S. Pawlowski, *Astrophys. J.* **836**, 152 (2017), [arXiv:1610.08981 \[astro-ph.GA\]](#).
- [18] H. Katz, F. Lelli, S. S. McGaugh, A. Di Cintio, C. B. Brook, and J. M. Schombert, *Mon. Not. Roy. Astron. Soc.* **466**, 1648 (2017), [arXiv:1605.05971 \[astro-ph.GA\]](#).
- [19] F. Lelli, S. S. McGaugh, and J. M. Schombert, *Mon. Not. Roy. Astron. Soc.* **468**, L68 (2017), [arXiv:1702.04355 \[astro-ph.GA\]](#).
- [20] H. Desmond, H. Katz, F. Lelli, and S. McGaugh, *Mon. Not. Roy. Astron. Soc.* **484**, 239 (2019), [arXiv:1808.00271 \[astro-ph.GA\]](#).
- [21] P. Li, F. Lelli, S. S. McGaugh, N. Starkman, and J. M. Schombert, *Mon. Not. Roy. Astron. Soc.* **482**, 5106 (2019), [arXiv:1811.00553 \[astro-ph.GA\]](#).
- [22] P. Li, F. Lelli, S. McGaugh, and J. Schombert, *Astron. Astrophys.* **615**, A3 (2018), [arXiv:1803.00022 \[astro-ph.GA\]](#).
- [23] H. Katz, H. Desmond, S. McGaugh, and F. Lelli, *Mon. Not. Roy. Astron. Soc.* **483**, L98 (2019), [arXiv:1810.12347 \[astro-ph.GA\]](#).
- [24] S. S. McGaugh, P. Li, F. Lelli, and J. M. Schombert, *Nature Astronomy* **2**, 924 (2018).
- [25] N. Starkman, F. Lelli, S. McGaugh, and J. Schombert, "Mon. Not. Roy. Astron. Soc." **480**, 2292 (2018), [arXiv:1802.09967 \[astro-ph.GA\]](#).
- [26] H. Katz, H. Desmond, F. Lelli, S. McGaugh, A. Di Cintio, C. Brook, and J. Schombert, "Mon. Not. Roy. Astron. Soc." **480**, 4287 (2018), [arXiv:1808.00971 \[astro-ph.GA\]](#).
- [27] P. Li, F. Lelli, S. McGaugh, M. S. Pawlowski, M. A. Zwaan, and J. Schombert, *Astrophys. J. Lett.* **886**, L11 (2019), [arXiv:1911.00517 \[astro-ph.GA\]](#).
- [28] S. McGaugh, F. Lelli, P. Li, and J. Schombert, in *IAU Symposium 353: Galactic Dynamics in the Era of Large Surveys* (2019) [arXiv:1909.02011 \[astro-ph.GA\]](#).
- [29] F. Lelli, S. S. McGaugh, J. M. Schombert, H. Desmond, and H. Katz, *Mon. Not. Roy. Astron. Soc.* **484**, 3267 (2019), [arXiv:1901.05966 \[astro-ph.GA\]](#).
- [30] J. Schombert, S. McGaugh, and F. Lelli, *Mon. Not. R. Astron. Soc.* **483**, 1496 (2019), [arXiv:1811.10579 \[astro-ph.GA\]](#).
- [31] L. Street, N. Y. Gnedin, and L. C. R. Wijewardhana, *Phys. Rev. D* **106**, 043007 (2022), [arXiv:2204.01871 \[astro-ph.CO\]](#).
- [32] J. F. Navarro, C. S. Frenk, and S. D. M. White, *Astrophys. J.* **490**, 493 (1997), [arXiv:astro-ph/9611107](#).
- [33] V. Springel, J. Wang, M. Vogelsberger, A. Ludlow, A. Jenkins, A. Helmi, J. F. Navarro, C. S. Frenk, and S. D. M. White, *Monthly Notices of the Royal Astronomical Society* **391**, 1685 (2008), [arXiv:0809.0898 \[astro-ph\]](#).
- [34] J. F. Navarro, A. Ludlow, V. Springel, J. Wang, M. Vogelsberger, S. D. M. White, A. Jenkins, C. S. Frenk, and A. Helmi, *Monthly Notices of the Royal Astronomical Society* **402**, 21 (2010), [arXiv:0810.1522 \[astro-ph\]](#).
- [35] H. Zhao, *Mon. Not. Roy. Astron. Soc.* **278**, 488 (1996), [arXiv:astro-ph/9509122](#).
- [36] N. W. Evans and J. An, *Monthly Notices of the Royal*

- Astronomical Society **360**, 492 (2005), [arXiv:astro-ph/0501091 \[astro-ph\]](#).
- [37] N. W. Evans and A. A. Williams, *Monthly Notices of the Royal Astronomical Society* **443**, 791 (2014), [arXiv:1406.3730 \[astro-ph.GA\]](#).
- [38] H.-N. Lin and X. Li, *Mon. Not. Roy. Astron. Soc.* **487**, 5679 (2019), [arXiv:1906.08419 \[astro-ph.GA\]](#).
- [39] K. Hayashi, M. Chiba, and T. Ishiyama, *Astrophys. J.* **904**, 45 (2020), [arXiv:2007.13780 \[astro-ph.GA\]](#).
- [40] D. Benisty, E. I. Guendelman, A. van de Venn, D. Vasak, J. Struckmeier, and H. Stoecker, *Eur. Phys. J. C* **82**, 264 (2022), [arXiv:2109.01052 \[astro-ph.CO\]](#).
- [41] A. van de Venn, D. Vasak, J. Kirsch, and J. Struckmeier, *Eur. Phys. J. C* **83**, 288 (2023), [arXiv:2211.11868 \[gr-qc\]](#).
- [42] J. Kirsch, D. Vasak, A. van de Venn, and J. Struckmeier, *Eur. Phys. J. C* **83**, 425 (2023), [arXiv:2303.01165 \[gr-qc\]](#).
- [43] M. Milgrom, *Astrophys. J.* **270**, 365 (1983).
- [44] J. Bekenstein and M. Milgrom, *Astrophys. J.* **286**, 7 (1984).
- [45] P. Kroupa, I. Banik, H. Haghi, A. H. Zonoozi, J. Dabringhausen, B. Javanmardi, O. Müller, X. Wu, and H. Zhao, *Nature Astron.* **2**, 925 (2018), [arXiv:1811.11754 \[astro-ph.GA\]](#).
- [46] R. B. Tully and J. R. Fisher, *Astron. Astrophys.* **54**, 661 (1977).
- [47] S. S. McGaugh, J. M. Schombert, G. D. Bothun, and W. J. G. de Blok, *Astrophys. J. Lett.* **533**, L99 (2000), [arXiv:astro-ph/0003001](#).
- [48] K.-H. Chae, F. Lelli, H. Desmond, S. S. McGaugh, P. Li, and J. M. Schombert, *Astrophys. J.* **904**, 51 (2020), [Erratum: *Astrophys. J.* 910, 81 (2021)], [arXiv:2009.11525 \[astro-ph.GA\]](#).
- [49] J. D. Bekenstein, *Phys. Rev. D* **70**, 083509 (2004), [Erratum: *Phys. Rev. D* 71, 069901 (2005)], [arXiv:astro-ph/0403694](#).
- [50] F. Piazza and C. Marinoni, *Phys. Rev. Lett.* **91**, 141301 (2003), [arXiv:hep-ph/0304228](#).
- [51] M. Khelashvili, A. Rudakovskiy, and S. Hossfelder, (2024), [arXiv:2401.10202 \[astro-ph.CO\]](#).
- [52] S. Capozziello, P. Jovanović, V. B. Jovanović, and D. Borka, *JCAP* **06**, 044 (2017), [arXiv:1702.03430 \[gr-qc\]](#).
- [53] A. O. F. de Almeida, L. Amendola, and V. Niro, *JCAP* **08**, 012 (2018), [arXiv:1805.11067 \[astro-ph.GA\]](#).
- [54] M. Crăciun and T. Harko, (2023), [arXiv:2311.16893 \[gr-qc\]](#).
- [55] J. Henrichs, M. Lembo, F. Iocco, and L. Amendola, *Phys. Rev. D* **104**, 043009 (2021), [arXiv:2010.15190 \[astro-ph.GA\]](#).
- [56] S. Capozziello, V. B. Jovanović, D. Borka, and P. Jovanović, (2020), [10.1016/j.dark.2020.100573, arXiv:2004.11557 \[gr-qc\]](#).
- [57] D. C. Rodrigues, A. Hernandez-Arboleda, and A. Wojnar, *Phys. Dark Univ.* **41**, 101230 (2023), [arXiv:2204.03762 \[astro-ph.GA\]](#).
- [58] P. D. Mannheim and J. G. O'Brien, *Phys. Rev. D* **85**, 124020 (2012), [arXiv:1011.3495 \[astro-ph.CO\]](#).
- [59] J. Oppenheim and A. Russo, (2024), [arXiv:2402.19459 \[gr-qc\]](#).
- [60] A. Chernin, P. Teerikorpi, and Y. Baryshev, (2000), [arXiv:astro-ph/0012021](#).
- [61] Y. Baryshev, A. Chernin, and P. Teerikorpi, (2000), [arXiv:astro-ph/0011528](#).
- [62] A. D. Chernin, D. I. Santiago, and A. S. Silbergleit, *Phys. Lett. A* **294**, 79 (2002), [arXiv:astro-ph/0106144](#).
- [63] Y. J. Kim, J. Kang, M. G. Lee, and I. S. Jang, *Astrophys. J.* **905**, 104 (2020), [arXiv:2010.01364 \[astro-ph.CO\]](#).
- [64] I. D. Karachentsev, A. D. Chernin, and P. Teerikorpi, *Astrofiz.* **46**, 399 (2003), [arXiv:astro-ph/0304250](#).
- [65] A. D. Chernin, I. D. Karachentsev, M. J. Valtonen, V. P. Dolgachev, L. M. Domozhilova, and D. I. Makarov, *Astron. Astrophys.* **415**, 19 (2004), [arXiv:astro-ph/0310048](#).
- [66] P. Teerikorpi, A. D. Chernin, and Y. V. Baryshev, *Astron. Astrophys.* **440**, 791 (2005), [arXiv:astro-ph/0506683](#).
- [67] A. D. Chernin, P. Teerikorpi, M. J. Valtonen, G. G. Byrd, V. P. Dolgachev, and L. M. Domozhilova, (2009), [arXiv:0902.3871 \[astro-ph.CO\]](#).
- [68] A. D. Chernin, P. Teerikorpi, and Y. V. Baryshev, *Astron. Astrophys.* **456**, 13 (2006), [arXiv:astro-ph/0603226](#).
- [69] S. Peirani and J. A. D. F. Pacheco, *Astron. Astrophys.* **488**, 845 (2008), [arXiv:0806.4245 \[astro-ph\]](#).
- [70] A. D. Chernin, I. D. Karachentsev, O. G. Nasonova, P. Teerikorpi, M. J. Valtonen, V. P. Dolgachev, L. M. Domozhilova, and G. G. Byrd, *Astron. Astrophys.* **520**, A104 (2010), [arXiv:1006.0555 \[astro-ph.CO\]](#).
- [71] P. Teerikorpi and A. D. Chernin, *Astron. Astrophys.* **516**, A93 (2010), [arXiv:1006.0066 \[astro-ph.CO\]](#).
- [72] A. D. Chernin, *Astron. Rep.* **59**, 474 (2015).
- [73] A. D. Chernin, N. V. Emelyanov, and I. D. Karachentsev, *Mon. Not. Roy. Astron. Soc.* **449**, 2069 (2015), [arXiv:1508.03485 \[astro-ph.CO\]](#).
- [74] A. Silbergleit and A. Chernin, *Kepler Problem in the Presence of Dark Energy, and the Cosmic Local Flow*, SpringerBriefs in Physics (Springer, 2019).
- [75] R. Nandra, A. N. Lasenby, and M. P. Hobson, *Mon. Not. Roy. Astron. Soc.* **422**, 2945 (2012), [arXiv:1104.4458 \[gr-qc\]](#).
- [76] D. Benisty, A.-C. Davis, and N. W. Evans, *Astrophys. J. Lett.* **953**, L2 (2023), [arXiv:2306.14963 \[astro-ph.CO\]](#).
- [77] D. Benisty, (2024), [arXiv:2401.09546 \[astro-ph.CO\]](#).
- [78] D. Benisty, J. Wagner, and D. Staicova, *Astron. Astrophys.* **683**, A83 (2024), [arXiv:2310.11488 \[astro-ph.CO\]](#).
- [79] T. Baker, D. Psaltis, and C. Skordis, *Astrophys. J.* **802**, 63 (2015), [arXiv:1412.3455 \[astro-ph.CO\]](#).
- [80] V. Pavlidou and T. N. Tomaras, *JCAP* **09**, 020 (2014), [arXiv:1310.1920 \[astro-ph.CO\]](#).
- [81] V. Pavlidou, N. Tetradis, and T. N. Tomaras, *JCAP* **05**, 017 (2014), [arXiv:1401.3742 \[astro-ph.CO\]](#).
- [82] D. Tanoglidis, V. Pavlidou, and T. Tomaras, *JCAP* **12**, 060 (2015), [arXiv:1412.6671 \[astro-ph.CO\]](#).
- [83] D. Brout *et al.*, *Astrophys. J.* **938**, 110 (2022), [arXiv:2202.04077 \[astro-ph.CO\]](#).
- [84] E. Abdalla *et al.*, *JHEAp* **34**, 49 (2022), [arXiv:2203.06142 \[astro-ph.CO\]](#).
- [85] O. Akarsu, E. O. Colgáin, A. A. Sen, and M. M. Sheikh-Jabbari, (2024), [arXiv:2402.04767 \[astro-ph.CO\]](#).
- [86] J. Binney and S. Tremaine, *Galactic Dynamics* (1988).
- [87] M. J. White, *Astron. Astrophys.* **367**, 27 (2001), [arXiv:astro-ph/0011495](#).
- [88] L. Hernquist, *Astrophys. J.* **356**, 359 (1990).
- [89] W. J. Handley, M. P. Hobson, and A. N. Lasenby,

- Mon. Not. Roy. Astron. Soc. **450**, L61 (2015), [arXiv:1502.01856 \[astro-ph.CO\]](#).
- [90] A. Lewis, (2019), [arXiv:1910.13970 \[astro-ph.IM\]](#).
- [91] J. P. Edwards, U. Gerber, C. Schubert, M. A. Trejo, and A. Weber, *PTEP* **2017**, 083A01 (2017), [arXiv:1706.09979 \[physics.atom-ph\]](#).
- [92] D. Pricopi, *Astrophys. Space Sci.* **361**, 277 (2016).
- [93] R. Mukherjee and S. Sounda, *Indian Journal of Physics* **92**, 197 (2018), [arXiv:1705.02444 \[physics.plasm-ph\]](#).
- [94] E. Cavan, I. Haranas, I. Gkigkitzis, and K. Cobbett, *Astrophys. Space Sci.* **365**, 36 (2020).
- [95] R. D'Agostino, K. Jusufi, and S. Capozziello, (2024), [arXiv:2404.01846 \[astro-ph.CO\]](#).
- [96] P. Teerikorpi, P. Heinämäki, P. Nurmi, A. D. Chernin, M. Einasto, M. Valtonen, and G. Byrd, *Astron. Astrophys.* **577**, A144 (2015), [arXiv:1503.02805 \[astro-ph.CO\]](#).
- [97] W. Wang, J. Han, M. Cautun, Z. Li, and M. N. Ishigaki, *Sci. China Phys. Mech. Astron.* **63**, 109801 (2020), [arXiv:1912.02599 \[astro-ph.GA\]](#).
- [98] R. B. Tully, H. Courtois, Y. Hoffman, and D. Pomarède, *Nature* **513**, 71 (2014), [arXiv:1409.0880 \[astro-ph.CO\]](#).
- [99] D. Pomarède, R. B. Tully, R. Graziani, H. M. Courtois, Y. Hoffman, and J. Lezmy, *Astrophys. J.* **897**, 133 (2020), [arXiv:2007.04414 \[astro-ph.CO\]](#).
- [100] L. Giani, C. Howlett, K. Said, T. Davis, and S. Vagnozzi, *JCAP* **01**, 071 (2024), [arXiv:2311.00215 \[astro-ph.CO\]](#).